Partially Bayesian active learning cubature for structural reliability analysis with extremely small failure probabilities

Chao Dang[a,*], Matthias G.R. Faes[b], Marcos A. Valdebenito[b], Pengfei Wei[c], Michael Beer[a,d,e]

[a] *Institute for Risk and Reliability, Leibniz University Hannover, Callinstr. 34, Hannover 30167, Germany*
[b] *Chair for Reliability Engineering, TU Dortmund University, Leonhard-Euler-Str. 5, Dortmund 44227, Germany*
[c] *School of Power and Energy, Northwestern Polytechnical University, Xi'an 710072, PR China*
[d] *Institute for Risk and Uncertainty, University of Liverpool, Liverpool L69 7ZF, United Kingdom*
[e] *International Joint Research Center for Resilient Infrastructure & International Joint Research Center for Engineering Reliability and Stochastic Mechanics, Tongji University, Shanghai 200092, PR China*

Abstract

The Bayesian failure probability inference (BFPI) framework provides a well-established Bayesian approach to quantifying our epistemic uncertainty about the failure probability resulting from a limited number of performance function evaluations. However, it is still challenging to perform Bayesian active learning of the failure probability by taking advantage of the BFPI framework. In this work, three Bayesian active learning methods are proposed under the name 'partially Bayesian active learning cubature' (PBALC), based on a cleaver use of the BFPI framework for structural reliability analysis, especially when small failure probabilities are involved. Since the posterior variance of the failure probability is computationally expensive to evaluate, the underlying idea is to exploit only the posterior mean of the failure probability to design two critical components for Bayesian active learning, i.e., the stopping criterion and the learning function. On this basis, three sets of stopping criteria and learning functions are proposed, resulting in the three proposed methods PBALC1, PBALC2 and PBALC3. Furthermore, the analytically intractable integrals involved in the stopping criteria are properly addressed from a numerical point of view. Five numerical examples are studied to demonstrate the performance of the three proposed methods. It is found empirically that the proposed methods can assess very small failure probabilities and significantly outperform several existing methods in terms of accuracy and efficiency.

Keywords: Structural reliability analysis, Small failure probability, Bayesian failure probability inference, Bayesian active learning, Stopping criterion, Learning function

1. Introduction

Structural reliability analysis plays a critical role in assessing the ability of engineering structures and mechanical systems to perform their expected functions of safety, serviceability, durability, etc. One of the central problems in probabilistic reliability analysis is the computation of the so-called failure probability:

$$P_f = \mathbb{P}\left(g(\boldsymbol{X})\right) = \int_{\mathcal{X}} I(g(\boldsymbol{x})) f_{\boldsymbol{X}}(\boldsymbol{x}) \mathrm{d}\boldsymbol{x}, \tag{1}$$

where $\boldsymbol{X} = [X_1, X_2, \cdots, X_d] \in \mathcal{U} \subseteq \mathbb{R}^d$ is a vector of d random variables with known joint probability density function (PDF) $f_{\boldsymbol{X}}(\boldsymbol{x})$; $g(\cdot) : \mathbb{R}^d \to \mathbb{R}$ is the performance function (also known as the limit state function), which takes a negative value when a failure occurs; $I(\cdot) : \mathbb{R} \to \{0, 1\}$ is the indicator function: $I(g(\boldsymbol{x})) = 1$ if $g(\boldsymbol{x}) < 0$ and $I(g(\boldsymbol{x})) = 0$ otherwise. For a typical reliability analysis problem in practice, it is most unlikely to be possible to obtain the solution of Eq. (1) analytically. This is because, for example, the performance function g has a complicated mathematical structure or is even an implicit function. Therefore, one has to resort to a numerical method.

Over the past few decades, various numerical methods have been developed to approximate the failure probability. Existing methods can be roughly divided into five categories: (1) stochastic simulation methods, (2) asymptotic approximation methods, (3) moment based methods, (4) probability conservation based methods and (5) surrogate-assisted methods. Stochastic simulation methods include direct Monte Carlo simulation (MCS) and its various variants (e.g., importance sampling [1, 2], subset simulation [3, 4], directional simulation [5, 6] and line sampling [7]). The MCS method is considered to be a universal reliability analysis method that is robust to the dimensionality and non-linearity of the problem at hand. However, it requires a significantly large number of g-function evaluations to evaluate a small failure probability. While other variants of MCS may have improved computational efficiency, they are still computationally prohibitive for many real-world problems and have limited applicability. Asymptotic approximation methods make use of asymptotic analysis to approxiamte the failure probability integral [8]. Two representatives of such methods are the first-order reliability method (FORM) [9] and second-order reliability method (SORM) [10]. These

*Corresponding author
Email address: chao.dang@irz.uni-hannover.de (Chao Dang)

methods have received considerable attention from researchers and practitioners and have shown to be efficient in many practical applications. Nevertheless, it is still challenging to apply FORM and SORM to problems with, e.g., strong nonlinearity and multiple failure regions. Moment based methods approximate the failure probability by estimating the probability distribution of the output variable of the g-function from knowledge of its statistical moments. Examples of such methods are the fourth-order moment methods [11, 12] and fractional moments based maximum entropy methods [13, 14]. Compared to FORM and SORM, they are more convenient to use because they do not require searching for the most probable point. However, moment based methods need to estimate the statistical moments using numerical integration techniques and assume the distribution type of the output variable of the performance function, making it difficult to assess the underlying numerical errors. Probability conservation based methods also aim to capture the probability distribution of the output variable of the g-function, but based on the principle of probability conservation without knowing its statistical moments. Such methods consist of the probability density evolution method [15, 16] and direct probability integral method [17, 18]. These methods have a sound theoretical basis, but depend on the partitioning of probability space in the numerical implementation, which becomes difficult in high dimensions. To reduce the computational cost, surrogate-assisted methods attempt to construct a simplified model as a substitute for the original performance function. A representative example in this group is the active learning Kriging methods [19, 20]. In fact, active learning methods have received a lot of attention in the reliability analysis community in the last decade.

More recently, the first author and his collaborators have developed a special class of active learning methods that emphasize the use of Bayesian principles. For convenience, we will refer to this type of methods as Bayesian active learning methods, although they may also have the characteristics of Bayesian probabilistic integration [21]. The reference [22] initialized the idea of turning the problem of the failure probability integral estimation into a Bayesian active learning problem. Specifically, a Bayesian approach was first developed to express our epistemic uncertainty about the true value of the failure probability resulting from a limited number of observations of the performance function. In this context, by assigning a Gaussian process prior over the performance function, the posterior mean and an upper bound of the

failure probability were derived in analytic form. Then, based on these posterior statistics of the failure probability, a learning function and a stopping criterion were proposed to facilitate active learning. The resulting method was called 'Active Learning Probabilistic Integration' (ALPI). It was further improved by the 'Parallel Adaptive Bayesian Quadrature' (PABQ) method [23] in order to estimate small failure probabilities and enable parallel computing. Note that the upper bound of the posterior variance may overestimate the true variance in most cases. The Bayesian approach developed in [22] was thus enriched by the 'Bayesian Failure Probability Inference' (BFPI) framework [24], where the exact expression of the posterior variance of the failure probability was derived. However, it is computationally prohibitive to use in an active learning context. As a compromise, we developed a Bayesian active learning method called 'Parallel Bayesian Probabilistic Integration' (PBPI) [25], in which a pseudo posterior variance inspired by the upper bound was proposed. In addition to these studies, the Bayesian active learning idea has also been successfully pursued in the context of line sampling, see for example [26, 27]. The Bayesian active learning paradigm has demonstrated many attractive features over several existing paradigms, including the active learning paradigm, but considerable effort is needed to make it an effective tool for practical reliability analysis.

The main objective of this work is to develop a novel Bayesian active learning method through a clever use of the BPFI framework [24] for assessing extremely small failure probabilities, which is one of main challenges in the context of structural reliability analysis. To achieve this goal, the key lies in developing the two critical components for Bayesian active learning from the posterior statistics of the failure probability, namely the stopping criterion and the learning function. Since the posterior variance of the failure probability is computationally expensive to evaluate, our key idea is to leverage only the posterior mean, in contrast to the previous studies [22, 23, 25] . On this basis, we first propose three new stopping criteria that can decide when to stop the active learning process. The intractable integrals involved are then tackled by a robust numerical integration scheme. In addition, three new learning functions are extracted from the proposed stopping criteria. These developments form three reliability methods under the name of 'Partially Bayesian Active Learning Cubature' (PBALC). The proposed methods are expected to further advance the use of

Bayesian active learning in the field of structural reliability analysis.

The rest of this paper is organized as follows. Section 2 is devoted to a general overview of the BFPI framework. The three proposed PBALC methods are introduced in section 3. Several numerical examples are examined in section 4 to demonstrate the performance of the proposed methods. Section 5 concludes the main findings of this study.

2. Bayesian failure probability inference

This section gives a brief overview of the BFPI framework developed in [24]. Note that the original framework is defined in the physical space, i.e., $\mathcal{X}$. Here it is presented in the standard normal space (denoted as $\mathcal{U}$) to facilitate the development of the proposed methods in the next section. To this end, we first introduce a transformed performance function $\mathcal{G}(\boldsymbol{U}) = g(T^{-1}(\boldsymbol{U}))$, where $\boldsymbol{U} = [U_1, U_2, \cdots, U_d] \in \mathcal{U} \subseteq \mathbb{R}^d$ is a vector of d independent standard normal variables and $T : \boldsymbol{U} = T(\boldsymbol{X})$ is an appropriate transformation that can transform the physical random vector $\boldsymbol{X}$ into the standard normal vector $\boldsymbol{U}$. The joint PDF of $\boldsymbol{U}$ is denoted as $\phi_{\boldsymbol{U}}(\boldsymbol{u})$.

2.1. Prior distribution

The essence of the BFPI framework is that the transformed performance function $\mathcal{G}(\cdot)$ should be treated as an unknown function. This is reasonable in the sense that very often the $\mathcal{G}$-function is complicated in its inner structure, and even is a black box in practical problems. Moreover, the value of the $\mathcal{G}$-function at a given location $\boldsymbol{u}$ is not even known until we actually evaluate it. To express our epistemic uncertainty, we can therefore formulate a prior distribution for the $\mathcal{G}$-function. Among many possible options, a Gaussian process (GP) prior can be adopted such that:

$$\mathcal{G}_0(\boldsymbol{u}) \sim \mathcal{GP}(m_{\mathcal{G}_0}(\boldsymbol{u}), k_{\mathcal{G}_0}(\boldsymbol{u}, \boldsymbol{u}')), \tag{2}$$

where $\mathcal{G}_0$ denotes the prior distribution of $\mathcal{G}$; $m_{\mathcal{G}_0}(\boldsymbol{u})$ and $k_{\mathcal{G}_0}(\boldsymbol{u}, \boldsymbol{u}')$ are the prior mean and covariance functions, respectively. Without loss of generality, the prior mean and covariance functions can be assumed

to a constant and a Gaussian kernel, receptively:

$$m_{\mathcal{G}_0}(\boldsymbol{u}) = \beta, \tag{3}$$

$$k_{\mathcal{G}_0}(\boldsymbol{u}, \boldsymbol{u}') = \sigma_0^2 \exp\left(-\frac{1}{2}(\boldsymbol{u} - \boldsymbol{u}')^\top \boldsymbol{\Sigma}^{-1}(\boldsymbol{u} - \boldsymbol{u}')\right), \tag{4}$$

where $\beta \in \mathbb{R}$; $\sigma_0 > 0$ is the standard deviation of the process; $\boldsymbol{\Sigma} = \text{diag}\left(l_1^2, l_2^2, \cdots, l_d^2\right)$ with $l_i > 0$ being the length scale in the i-th dimension. The $d + 2$ parameters collected in $\boldsymbol{\vartheta} = [\beta, \sigma_0, l_1, l_2, \cdots, l_d]$ are referred to as hyperparameters.

2.2. Estimating hyperparameters

Suppose that now we have an observation dataset $\boldsymbol{\mathcal{D}} = \{\boldsymbol{\mathcal{U}}, \boldsymbol{\mathcal{Y}}\}$, where $\boldsymbol{\mathcal{U}} = \left\{\boldsymbol{u}^{(j)}\right\}_{j=1}^{n}$ is an $n \times d$ matrix with its j-th row being $\boldsymbol{u}^{(j)}$ and $\boldsymbol{\mathcal{Y}} = \left[y^{(1)}, y^{(2)}, \cdots, y^{(n)}\right]^\top$ is an $n \times 1$ vector with its j-th element being $y^{(j)} = \mathcal{G}(\boldsymbol{u}^{(j)})$. The hyperparameters in $\boldsymbol{\vartheta}$ can be specified by maximizing the log-marginal likelihood:

$$\log p(\boldsymbol{\mathcal{Y}}|\boldsymbol{\mathcal{U}}, \boldsymbol{\vartheta}) = -\frac{1}{2}\left[(\boldsymbol{\mathcal{Y}} - \beta)^\top \boldsymbol{K}_{\mathcal{G}_0}^{-1}(\boldsymbol{\mathcal{Y}} - \beta) + \log|\boldsymbol{K}_{\mathcal{G}_0}| + n\log 2\pi\right], \tag{5}$$

where $\boldsymbol{K}_{\mathcal{G}_0}$ is an $n \times n$ covariance matrix with (i, j)-th entry being $k_{\mathcal{G}_0}(\boldsymbol{u}^{(i)}, \boldsymbol{u}^{(j)})$.

2.3. Posterior statistics

The posterior distribution of $\mathcal{G}$ conditional on the data $\boldsymbol{\mathcal{D}}$ is again a GP:

$$\mathcal{G}_n(\boldsymbol{u}) \sim \mathcal{GP}(m_{\mathcal{G}_n}(\boldsymbol{u}), k_{\mathcal{G}_n}(\boldsymbol{u}, \boldsymbol{u}')), \tag{6}$$

where $\mathcal{G}_n$ stands for the posterior distribution of $\mathcal{G}$ after seeing n observations; $m_{\mathcal{G}_n}(\boldsymbol{u})$ and $k_{\mathcal{G}_n}(\boldsymbol{u}, \boldsymbol{u}')$ are the posterior mean and covariance functions respectively, which can be expressed as:

$$m_{\mathcal{G}_n}(\boldsymbol{u}) = m_{\mathcal{G}_0}(\boldsymbol{u}) + \boldsymbol{k}_{\mathcal{G}_0}(\boldsymbol{u}, \boldsymbol{\mathcal{U}})^\top \boldsymbol{K}_{\mathcal{G}_0}^{-1}\left(\boldsymbol{\mathcal{Y}} - \boldsymbol{m}_{\mathcal{G}_0}(\boldsymbol{\mathcal{U}})\right), \tag{7}$$

$$k_{\mathcal{G}_n}(\boldsymbol{u}, \boldsymbol{u}') = k_{\mathcal{G}_0}(\boldsymbol{u}, \boldsymbol{u}') - \boldsymbol{k}_{\mathcal{G}_0}(\boldsymbol{u}, \boldsymbol{\mathcal{U}})^\top \boldsymbol{K}_{\mathcal{G}_0}^{-1} \boldsymbol{k}_{\mathcal{G}_0}(\boldsymbol{\mathcal{U}}, \boldsymbol{u}'), \tag{8}$$

in which $\boldsymbol{m}_{\mathcal{G}_0}(\boldsymbol{\mathcal{U}})$ is an $n \times 1$ mean vector with j-th element being $m_{\mathcal{G}_0}(\boldsymbol{u}^{(j)})$; $\boldsymbol{k}_{\mathcal{G}_0}(\boldsymbol{u}, \boldsymbol{\mathcal{U}})$ and $\boldsymbol{k}_{\mathcal{G}_0}(\boldsymbol{\mathcal{U}}, \boldsymbol{u}')$ are two $n \times 1$ covariance vectors with j-th element being $k_{\mathcal{G}_0}(\boldsymbol{u}, \boldsymbol{u}^{(j)})$ and $k_{\mathcal{G}_0}(\boldsymbol{u}^{(j)}, \boldsymbol{u}')$, respectively.

Through some mathematical derivation, we can obtain the posterior mean and variance of the failure probability:

$$m_{P_{f,n}} = \int_{\mathcal{U}} \Phi\left(-\frac{m_{\mathcal{G}_n}(\boldsymbol{u})}{\sigma_{\mathcal{G}_n}(\boldsymbol{u})}\right) \phi_{\boldsymbol{U}}(\boldsymbol{u}) \mathrm{d}\boldsymbol{u}, \tag{9}$$

$$\sigma^2_{P_{f,n}} = \int_{\mathcal{U}}\int_{\mathcal{U}} \left[\Phi_2\left([0,0]^\top; \boldsymbol{m}_{\mathcal{G}_n}(\boldsymbol{u},\boldsymbol{u}'), \boldsymbol{K}_{\mathcal{G}_n}(\boldsymbol{u},\boldsymbol{u}')\right) - \Phi\left(\frac{-m_{\mathcal{G}_n}(\boldsymbol{u})}{\sigma_{\mathcal{G}_n}(\boldsymbol{u})}\right)\Phi\left(\frac{-m_{\mathcal{G}_n}(\boldsymbol{u}')}{\sigma_{\mathcal{G}_n}(\boldsymbol{u}')}\right)\right] \phi_{\boldsymbol{U}}(\boldsymbol{u})\phi_{\boldsymbol{U}}(\boldsymbol{u}') \mathrm{d}\boldsymbol{u}\mathrm{d}\boldsymbol{u}', \tag{10}$$

where $P_{f,n}$ denotes the posterior distribution of the failure probability P_f conditional on $\boldsymbol{\mathcal{D}}$; Φ is the cumulative distribution function (CDF) of the standard normal variable; $\sigma_{\mathcal{G}_n}(\boldsymbol{u})$ is the posterior standard deviation function of $\mathcal{G}$, i.e., $\sigma_{\mathcal{G}_n}(\boldsymbol{u}) = \sqrt{k_{\mathcal{G}_n}(\boldsymbol{u},\boldsymbol{u})}$; Φ_2 denotes the bivariate normal CDF, which is not analytically available; $\boldsymbol{m}_{\mathcal{G}_n}(\boldsymbol{u},\boldsymbol{u}')$ is the posterior mean vector of $\mathcal{G}$, i.e., $\boldsymbol{m}_{\mathcal{G}_n}(\boldsymbol{u},\boldsymbol{u}') = [m_{\mathcal{G}_n}(\boldsymbol{u}), m_{\mathcal{G}_n}(\boldsymbol{u}')]^\top$; $\boldsymbol{K}_{\mathcal{G}_n}(\boldsymbol{u},\boldsymbol{u}')$ is the posterior covariance matrix of $\mathcal{G}$:

$$\boldsymbol{K}_{\mathcal{G}_n}(\boldsymbol{u},\boldsymbol{u}') = \begin{bmatrix} \sigma^2_{\mathcal{G}_n}(\boldsymbol{u}) & k_{\mathcal{G}_n}(\boldsymbol{u}',\boldsymbol{u}) \\ k_{\mathcal{G}_n}(\boldsymbol{u},\boldsymbol{u}') & \sigma^2_{\mathcal{G}_n}(\boldsymbol{u}') \end{bmatrix}. \tag{11}$$

The posterior distribution $P_{f,n}$ provides a probabilistic descriptor for our uncertainty about the true value of the failure probability P_f. This uncertainty arises from the fact that the $\mathcal{G}$-function is only observed at a finite number of discrete locations. Although the analytical solution of $P_{f,n}$ is not yet known, several numerical investigations in [24] suggest that it can be well approximated by a normal distribution $\mathcal{N}(m_{P_{f,n}}, \sigma^2_{P_{f,n}})$. In fact, one may be more interested in the posterior mean and variance of the failure probability than its full distribution in practical applications. This is because that the posterior mean $m_{P_{f,n}}$ can be used as a failure probability predictor, while the posterior variance $\sigma^2_{P_{f,n}}$ can provide a measure of the prediction uncertainty. Note, however, that both $m_{P_{f,n}}$ and $\sigma^2_{P_{f,n}}$ cannot be solved analytically, and a numerical integrator must be used. Compared to $m_{P_{f,n}}$, $\sigma^2_{P_{f,n}}$ is much harder to approximate numerically due to its underlying complexity.

3. Partially Bayesian active learning cubature

In this section, we further frame the failure probability estimation in a Bayesian active learning setting based on the BFPI framework. To achieve this, the key is to develop two crucial components: stopping

criterion and learning function. The stopping criterion is used to determine when to stop the learning process, while the learning function is used to suggest where to evaluate the $\mathcal{G}$-function if the stopping criterion is not met. Therefore, they both can significantly affect the performance of the resulting method. Our basic idea is to use only the posterior mean of the failure probability to construct the stopping criterion and the learning function because the posterior variance is not easy to handle from a numerical perspective. Along this line of thought, three sets of learning functions and stopping criteria are creatively proposed, leading to three novel methods, called PBALC1, PBALC2 and PBALC3.

3.1. Three stopping criteria

The posterior mean of the failure probability ($m_{P_{f,n}}$ defined in Eq. (9)) represents the updated average value of the failure probability, given both some observed data $\boldsymbol{\mathcal{D}}$ and a GP prior of the $\mathcal{G}$-function. Therefore, it alone cannot give any information about its accuracy as a predictor of the failure probability. However, it is still possible to make strategic use of the structure of $m_{P_{f,n}}$ to construct a measure of the accuracy of our predictor.

Note that the integrand of $m_{P_{f,n}}$ involves a term $\Phi\left(-\frac{m_{\mathcal{G}_n}(\boldsymbol{u})}{\sigma_{\mathcal{G}_n}(\boldsymbol{u})}\right)$, which is related to both the posterior mean and standard derivation functions of $\mathcal{G}$. If $m_{\mathcal{G}_n}(\boldsymbol{u})$ on the numerator is replaced by the upper and lower credible bounds of $\mathcal{G}_n$, then we can define two new quantities:

$$\begin{aligned}\underline{m}_{P_{f,n}} &= \int_{\mathcal{U}} \Phi\left(-\frac{m_{\mathcal{G}_n}(\boldsymbol{u}) + b\sigma_{\mathcal{G}_n}(\boldsymbol{u})}{\sigma_{\mathcal{G}_n}(\boldsymbol{u})}\right)\phi_{\boldsymbol{U}}(\boldsymbol{u})\mathrm{d}\boldsymbol{u} \\ &= \int_{\mathcal{U}} \Phi\left(-\frac{m_{\mathcal{G}_n}(\boldsymbol{u})}{\sigma_{\mathcal{G}_n}(\boldsymbol{u})} - b\right)\phi_{\boldsymbol{U}}(\boldsymbol{u})\mathrm{d}\boldsymbol{u},\end{aligned} \tag{12}$$

$$\begin{aligned}\overline{m}_{P_{f,n}} &= \int_{\mathcal{U}} \Phi\left(-\frac{m_{\mathcal{G}_n}(\boldsymbol{u}) - b\sigma_{\mathcal{G}_n}(\boldsymbol{u})}{\sigma_{\mathcal{G}_n}(\boldsymbol{u})}\right)\phi_{\boldsymbol{U}}(\boldsymbol{u})\mathrm{d}\boldsymbol{u} \\ &= \int_{\mathcal{U}} \Phi\left(-\frac{m_{\mathcal{G}_n}(\boldsymbol{u})}{\sigma_{\mathcal{G}_n}(\boldsymbol{u})} + b\right)\phi_{\boldsymbol{U}}(\boldsymbol{u})\mathrm{d}\boldsymbol{u},\end{aligned} \tag{13}$$

where $0 < b < \infty$ implies that $[m_{\mathcal{G}_n}(\boldsymbol{u}) - b\sigma_{\mathcal{G}_n}(\boldsymbol{u}), m_{\mathcal{G}_n}(\boldsymbol{u}) + b\sigma_{\mathcal{G}_n}(\boldsymbol{u})]$ is a $100(1-2\Phi(-b))\%$ credible bound of $\mathcal{G}_n$. We have the following proposition:

Proposition 1. *For $b > 0$, there exists $\underline{m}_{P_{f,n}} < m_{P_{f,n}} < \overline{m}_{P_{f,n}}$.*

Proof. We first prove that the first inequality $\underline{m}_{P_{f,n}} < m_{P_{f,n}}$ holds true. For this purpose, the following equation is given:

$$\begin{aligned} \underline{m}_{P_{f,n}} - m_{P_{f,n}} &= \int_{\mathcal{U}} \Phi\left(-\frac{m_{\mathcal{G}_n}(\boldsymbol{u})}{\sigma_{\mathcal{G}_n}(\boldsymbol{u})} - b\right) \phi_{\boldsymbol{U}}(\boldsymbol{u})\mathrm{d}\boldsymbol{u} - \int_{\mathcal{U}} \Phi\left(-\frac{m_{\mathcal{G}_n}(\boldsymbol{u})}{\sigma_{\mathcal{G}_n}(\boldsymbol{u})}\right) \phi_{\boldsymbol{U}}(\boldsymbol{u})\mathrm{d}\boldsymbol{u} \\ &= \int_{\mathcal{U}} \left[\Phi\left(-\frac{m_{\mathcal{G}_n}(\boldsymbol{u})}{\sigma_{\mathcal{G}_n}(\boldsymbol{u})} - b\right) - \Phi\left(-\frac{m_{\mathcal{G}_n}(\boldsymbol{u})}{\sigma_{\mathcal{G}_n}(\boldsymbol{u})}\right)\right] \phi_{\boldsymbol{U}}(\boldsymbol{u})\mathrm{d}\boldsymbol{u}. \end{aligned} \tag{14}$$

Recall that Φ is a monotonically increasing function and $\phi_{\boldsymbol{U}}(\boldsymbol{u}) > 0$ for $\forall \boldsymbol{u} \in \mathcal{U}$. Under the condition $b > 0$, we have the following inequality:

$$\left[\Phi\left(-\frac{m_{\mathcal{G}_n}(\boldsymbol{u})}{\sigma_{\mathcal{G}_n}(\boldsymbol{u})} - b\right) - \Phi\left(-\frac{m_{\mathcal{G}_n}(\boldsymbol{u})}{\sigma_{\mathcal{G}_n}(\boldsymbol{u})}\right)\right] \phi_{\boldsymbol{U}}(\boldsymbol{u}) < 0. \tag{15}$$

Combining Eq. (14) and inequality (15) leads to $\underline{m}_{P_{f,n}} - m_{P_{f,n}} < 0$. Hence, $\underline{m}_{P_{f,n}} < m_{P_{f,n}}$ is proved.

Analogous to the proof of the first inequality, the second inequality $m_{P_{f,n}} < \overline{m}_{P_{f,n}}$ can also be proved. Combining $\underline{m}_{P_{f,n}} < m_{P_{f,n}}$ and $m_{P_{f,n}} < \overline{m}_{P_{f,n}}$ completes the proof. □

Proposition 1 suggests that as long as $b > 0$, $m_{P_{f,n}}$ is always larger than $\underline{m}_{P_{f,n}}$ and smaller than $\overline{m}_{P_{f,n}}$. Therefore, we shall refer to $\underline{m}_{P_{f,n}}$ as the 'left-shifted posterior mean (LSPM) of the failure probability', and to $\overline{m}_{P_{f,n}}$ as the 'right-shifted posterior mean (RSPM) of the failure probability'. One might be interested in the asymptotic properties of $\underline{m}_{P_{f,n}}$, $m_{P_{f,n}}$ and $\overline{m}_{P_{f,n}}$. We first give the asymptotic property of $m_{P_{f,n}}$ by the following proposition:

Proposition 2. *When $\sigma_{\mathcal{G}_n}(\boldsymbol{u}) \to 0^+$ and $m_{\mathcal{G}_n}(\boldsymbol{u}) \to \mathcal{G}(\boldsymbol{u})$, there exists $m_{P_{f,n}} \to P_f$.*

Proof. In case that $\sigma_{\mathcal{G}_n}(\boldsymbol{u}) \to 0^+$ and $m_{\mathcal{G}_n}(\boldsymbol{u}) \to \mathcal{G}(\boldsymbol{u})$, it is easy to show that:

$$\Phi\left(-\frac{m_{\mathcal{G}_n}(\boldsymbol{u})}{\sigma_{\mathcal{G}_n}(\boldsymbol{u})}\right) \to I(\mathcal{G}(\boldsymbol{u})), \tag{16}$$

where

$$I(\mathcal{G}(\boldsymbol{u})) = \begin{cases} 1, \mathcal{G}(\boldsymbol{u}) < 0 \\ 0, \text{otherwise} \end{cases}. \tag{17}$$

It follows immediately that

$$m_{P_{f,n}} = \int_{\mathcal{U}} \Phi\left(-\frac{m_{\mathcal{G}_n}(\boldsymbol{u})}{\sigma_{\mathcal{G}_n}(\boldsymbol{u})}\right) \phi_{\boldsymbol{U}}(\boldsymbol{u})\mathrm{d}\boldsymbol{u} \to P_f = \int_{\mathcal{U}} I(\mathcal{G}(\boldsymbol{u}))\phi_{\boldsymbol{U}}(\boldsymbol{u})\mathrm{d}\boldsymbol{u}. \tag{18}$$

This completes the proof. □

Proposition 2 implies that the failure probability predictor $m_{P_{f,n}}$ can theoretically approach the true value of the failure probability. The asymptotic properties of $\underline{m}_{P_{f,n}}$ and $\overline{m}_{P_{f,n}}$ can be given by the following proposition:

Proposition 3. *When* $\sigma_{\mathcal{G}_n}(\boldsymbol{u}) \to 0^+$, $m_{\mathcal{G}_n}(\boldsymbol{u}) \to \mathcal{G}(\boldsymbol{u})$ *and* $0 < b < \infty$, *there exist* $\underline{m}_{P_{f,n}} \to m^-_{P_{f,n}}$ *and* $\overline{m}_{P_{f,n}} \to m^+_{P_{f,n}}$.

Proof. We first prove that $\underline{m}_{P_{f,n}} \to m^-_{P_{f,n}}$ holds true. Given that $\sigma_{\mathcal{G}_n}(\boldsymbol{u}) \to 0^+$, $m_{\mathcal{G}_n}(\boldsymbol{u}) \to \mathcal{G}(\boldsymbol{u})$ and $0 < b < \infty$, it is easy to know that

$$\Phi\left(-\frac{m_{\mathcal{G}_n}(\boldsymbol{u})}{\sigma_{\mathcal{G}_n}(\boldsymbol{u})} - b\right) \to \Phi\left(-\frac{m_{\mathcal{G}_n}(\boldsymbol{u})}{\sigma_{\mathcal{G}_n}(\boldsymbol{u})}\right)^- . \tag{19}$$

Then it follows immediately that:

$$\underline{m}_{P_{f,n}} = \int_{\mathcal{U}} \Phi\left(-\frac{m_{\mathcal{G}_n}(\boldsymbol{u})}{\sigma_{\mathcal{G}_n}(\boldsymbol{u})} - b\right) \phi_{\boldsymbol{U}}(\boldsymbol{u}) \mathrm{d}\boldsymbol{u} \to m^-_{P_{f,n}} = \int_{\mathcal{U}} \Phi\left(-\frac{m_{\mathcal{G}_n}(\boldsymbol{u})}{\sigma_{\mathcal{G}_n}(\boldsymbol{u})}\right) \phi_{\boldsymbol{U}}(\boldsymbol{u}) \mathrm{d}\boldsymbol{u} \tag{20}$$

Therefore, $\underline{m}_{P_{f,n}} \to m^-_{P_{f,n}}$ is proved.

Analogous to the proof of $\underline{m}_{P_{f,n}} \to m^-_{P_{f,n}}$, $\overline{m}_{P_{f,n}} \to m^+_{P_{f,n}}$ can also be proved. Combing these results completes the proof of the proposition. □

Proposition 3 indicates that the LSPM of the failure probability $\underline{m}_{P_{f,n}}$ will approach to the posterior mean $m_{P_{f,n}}$ from the left and the RSPM of the failure probability $\overline{m}_{P_{f,n}}$ will approach to the posterior mean $m_{P_{f,n}}$ from the right when the GP posterior approaches to the $\mathcal{G}$-function. In the meantime, the posterior mean of the failure probability $m_{P_{f,n}}$ will approach to the true failure probability P_f as reflected by proposition 2. Despite the inclusion of the harsh condition (i.e., $\sigma_{\mathcal{G}_n}(\boldsymbol{u}) \to 0^+$ and $m_{\mathcal{G}_n}(\boldsymbol{u}) \to \mathcal{G}(\boldsymbol{u})$), propositions 2 and 3 will provide us with a sound basis for developing the stopping criteria and even the learning functions.

In this study, we propose the following three stopping criteria:

$$\text{Stopping criterion 1: } \frac{m_{P_{f,n}} - \underline{m}_{P_{f,n}}}{m_{P_{f,n}}} < \epsilon_1, \tag{21}$$

$$\text{Stopping criterion 2: } \frac{\overline{m}_{P_{f,n}} - m_{P_{f,n}}}{m_{P_{f,n}}} < \epsilon_2, \tag{22}$$

$$\text{Stopping criterion 3: } \frac{\overline{m}_{P_{f,n}} - \underline{m}_{P_{f,n}}}{m_{P_{f,n}}} < \epsilon_3, \tag{23}$$

where ϵ_1, ϵ_2 and ϵ_3 are three user-specified tolerances. Stopping criterion 1 means that the learning process is terminated when the relative difference between $m_{P_{f,n}}$ and $\underline{m}_{P_{f,n}}$ falls below a certain threshold ϵ_1. The other two stopping criteria can also be interpreted similarly. It should be emphasized that the three stopping criteria have a parsimonious form and their validity is theoretically guaranteed. Implementing the above three stopping criteria, however, requires the treatment of the analytically intractable integrals involved. In this study, we employ the variance-amplified importance sampling (VAIS) technique developed in [24] in a sequential manner.

Taking stopping criterion 1 as an example, we have to approximate two integrals $m_{P_{f,n}}$ and $m_{P_{f,n}} - \underline{m}_{P_{f,n}}$. For notational simplicity, let $\underline{\Delta}_{P_{f,n}} = m_{P_{f,n}} - \underline{m}_{P_{f,n}}$. The VAIS estimators of $m_{P_{f,n}}$ and $\underline{\Delta}_{P_{f,n}}$ can be expressed as:

$$\hat{m}_{P_{f,n}} = \frac{1}{N}\sum_{i=1}^{N} \Phi\left(-\frac{m_{\mathcal{G}_n}(\boldsymbol{u}^{(i)})}{\sigma_{\mathcal{G}_n}(\boldsymbol{u}^{(i)})}\right) \frac{\phi_{\boldsymbol{U}}(\boldsymbol{u}^{(i)})}{h(\boldsymbol{u}^{(i)})}, \tag{24}$$

$$\hat{\underline{\Delta}}_{P_{f,n}} = \frac{1}{N}\sum_{i=1}^{N} \left[\Phi\left(-\frac{m_{\mathcal{G}_n}(\boldsymbol{u}^{(i)})}{\sigma_{\mathcal{G}_n}(\boldsymbol{u}^{(i)})}\right) - \Phi\left(-\frac{m_{\mathcal{G}_n}(\boldsymbol{u}^{(i)})}{\sigma_{\mathcal{G}_n}(\boldsymbol{u}^{(i)})} - b\right)\right] \frac{\phi_{\boldsymbol{U}}(\boldsymbol{u}^{(i)})}{h(\boldsymbol{u}^{(i)})}, \tag{25}$$

where $h(\boldsymbol{u})$ is the sampling density, which is equal to the joint PDF of n independent normal variables with a mean of zero and a standard deviation of $\lambda > 1$; $\left\{\boldsymbol{u}^{(i)}\right\}_{i=1}^{N}$ is a set of N random samples generated from $h(\boldsymbol{u})$. The variances associated with $\hat{m}_{P_{f,n}}$ and $\hat{\underline{\Delta}}_{P_{f,n}}$ are given by:

$$\mathbb{V}\left[\hat{m}_{P_{f,n}}\right] = \frac{1}{N-1}\left\{\frac{1}{N}\sum_{i=1}^{N}\left[\Phi\left(-\frac{m_{\mathcal{G}_n}(\boldsymbol{u}^{(i)})}{\sigma_{\mathcal{G}_n}(\boldsymbol{u}^{(i)})}\right)\frac{\phi_{\boldsymbol{U}}(\boldsymbol{u}^{(i)})}{h(\boldsymbol{u}^{(i)})}\right]^2 - \hat{m}^2_{P_{f,n}}\right\}, \tag{26}$$

$$\mathbb{V}\left[\underline{\Delta}_{P_{f,n}}\right] = \frac{1}{N-1}\left\{\frac{1}{N}\sum_{i=1}^{N}\left[\left(\Phi\left(-\frac{m_{\mathcal{G}_n}(\boldsymbol{u}^{(i)})}{\sigma_{\mathcal{G}_n}(\boldsymbol{u}^{(i)})}\right) - \Phi\left(-\frac{m_{\mathcal{G}_n}(\boldsymbol{u}^{(i)})}{\sigma_{\mathcal{G}_n}(\boldsymbol{u}^{(i)})} - b\right)\right)\frac{\phi_{\boldsymbol{U}}(\boldsymbol{u}^{(i)})}{h(\boldsymbol{u}^{(i)})}\right]^2 - \underline{\Delta}^2_{P_{f,n}}\right\}. \tag{27}$$

To speed up the computation and avoid the computer memory problem when a large N must be used, the VAIS method should be implemented sequentially. Moreover, we can also reuse information in the sequential process. The details of the algorithm are briefly explained as follows. Assume that the sample size is the same for each batch, say N_0. At the j-th iteration, first generate N_0 random samples from $h(\boldsymbol{u})$,

denoted as $\left\{\boldsymbol{u}^{(i)}\right\}_{i=1}^{N_0}$. Then, evaluate the following two terms:

$$q^{(i)} = -\frac{m_{\mathcal{G}_n}(\boldsymbol{u}^{(i)})}{\sigma_{\mathcal{G}_n}(\boldsymbol{u}^{(i)})}, \tag{28}$$

$$p^{(i)} = \frac{\phi_{\boldsymbol{U}}(\boldsymbol{u}^{(i)})}{h(\boldsymbol{u}^{(i)})}. \tag{29}$$

After that, we evaluate the following four terms:

$$\hat{m}_{P_{f,n}}^{(j)} = \frac{1}{N_0}\sum_{i=1}^{N_0} \Phi\left(q^{(i)}\right) p^{(i)}, \tag{30}$$

$$\hat{\underline{\Delta}}_{P_{f,n}}^{(j)} = \frac{1}{N_0}\sum_{i=1}^{N_0} \left(\Phi\left(q^{(i)}\right) - \Phi\left(q^{(i)} - b\right)\right) p^{(i)}, \tag{31}$$

$$s^{(j)} = \frac{1}{N_0}\sum_{i=1}^{N_0} \left[\Phi\left(q^{(i)}\right) p^{(i)}\right]^2, \tag{32}$$

$$r^{(j)} = \frac{1}{N_0}\sum_{i=1}^{N_0} \left[\left(\Phi\left(q^{(i)}\right) - \Phi\left(q^{(i)} - b\right)\right) p^{(i)}\right]^2. \tag{33}$$

Up to the j-th iteration, the estimates and variances for $m_{P_{f,n}}$ and $\underline{\Delta}_{P_{f,n}}$ can be calculated as follows:

$$\hat{m}_{P_{f,n}} = \frac{1}{j}\sum_{t=1}^{j} \hat{m}_{P_{f,n}}^{(t)}, \tag{34}$$

$$\hat{\underline{\Delta}}_{P_{f,n}} = \frac{1}{j}\sum_{t=1}^{j} \hat{\underline{\Delta}}_{P_{f,n}}^{(t)}, \tag{35}$$

$$\mathbb{V}\left[\hat{m}_{P_{f,n}}\right] = \frac{1}{jN_0 - 1}\left[\frac{1}{j}\sum_{t=1}^{j} s^{(t)} - \hat{m}_{P_{f,n}}^2\right], \tag{36}$$

$$\mathbb{V}\left[\underline{\Delta}_{P_{f,n}}\right] = \frac{1}{jN_0 - 1}\left[\frac{1}{j}\sum_{t=1}^{j} r^{(t)} - \underline{\Delta}_{P_{f,n}}^2\right]. \tag{37}$$

The above sequential process is repeated until a stopping criterion is satisfied, i.e., $\sqrt{\mathbb{V}\left[\hat{m}_{P_{f,n}}\right]}/\hat{m}_{P_{f,n}} < \delta_1$ and $\sqrt{\mathbb{V}\left[\hat{\underline{\Delta}}_{P_{f,n}}\right]}/\hat{\underline{\Delta}}_{P_{f,n}} < \delta_2$, where δ_1 and δ_2 are two user-defined thresholds. Note that the most time-consuming part is usually associated with the term $q^{(i)}$. Nevertheless, it can be reused in several places to reduce the overall computation time. This advantage comes mainly from the structure of the stopping criterion 1 that we propose. After the sequential VAIS procedure is completed, the numerator and denominator on the left-hand side of stopping criterion 1 should be replaced with their respective

estimates. Also, the stopping criterion is thus required to be satisfied twice in a row to avoid possible spurious convergence.

The other two stopping criteria (i.e., stopping criteria 2 and 3) can also be handled similarly to stopping criterion 1, and the computational benefits can also be reserved. Note that it is not necessary to use all three stopping criteria at the same time, but only one of them. The stopping criteria proposed in Eqs. (21) - (23) depend on the thresholds ϵ_1, ϵ_2 and ϵ_3 respectively, and also on the parameter b. If a smaller b is chosen, we need to set a smaller threshold to ensure the accuracy of the failure probability estimate and vice versa.

3.2. Three learning functions

A point at which the $\mathcal{G}$-function is evaluated next should be identified if the selected stopping criterion is not satisfied. This can usually be achieved by using a so-called learning (or acquisition) function. An appropriate learning function should be able to suggest promising points that cause the posterior mean of the failure probability to approach the true one, taking into account the trade-off between exploration and exploitation.

In this study, according to the three stopping criteria we propose the following three learning functions, which are called 'left-shifted contribution' (LSC), 'right-shifted contribution' (RSC) and 'left-shifted and right-shifted contribution' (LSRSC), respectively:

$$\text{Learning function 1: LSC}(\boldsymbol{u}) = \left[\Phi\left(-\frac{m_{\mathcal{G}_n}(\boldsymbol{u})}{\sigma_{\mathcal{G}_n}(\boldsymbol{u})}\right) - \Phi\left(-\frac{m_{\mathcal{G}_n}(\boldsymbol{u})}{\sigma_{\mathcal{G}_n}(\boldsymbol{u})} - b\right)\right]\phi_{\boldsymbol{U}}(\boldsymbol{u}), \tag{38}$$

$$\text{Learning function 2: RSC}(\boldsymbol{u}) = \left[\Phi\left(-\frac{m_{\mathcal{G}_n}(\boldsymbol{u})}{\sigma_{\mathcal{G}_n}(\boldsymbol{u})} + b\right) - \Phi\left(-\frac{m_{\mathcal{G}_n}(\boldsymbol{u})}{\sigma_{\mathcal{G}_n}(\boldsymbol{u})}\right)\right]\phi_{\boldsymbol{U}}(\boldsymbol{u}), \tag{39}$$

$$\text{Learning function 3: LSRSC}(\boldsymbol{u}) = \left[\Phi\left(-\frac{m_{\mathcal{G}_n}(\boldsymbol{u})}{\sigma_{\mathcal{G}_n}(\boldsymbol{u})} + b\right) - \Phi\left(-\frac{m_{\mathcal{G}_n}(\boldsymbol{u})}{\sigma_{\mathcal{G}_n}(\boldsymbol{u})} - b\right)\right]\phi_{\boldsymbol{U}}(\boldsymbol{u}). \tag{40}$$

Take learning function 1 as an example. Note that $m_{P_{f,n}} - \underline{m}_{P_{f,n}} = \int_{\mathcal{U}} \text{LSC}(\boldsymbol{u})\mathrm{d}\boldsymbol{u}$ holds. The learning function $\text{LSC}(\boldsymbol{u})$ can thus be interpreted as a measure of the contribution at the point $\boldsymbol{u}$ to the difference between the posterior mean and the left-shifted posterior mean of the failure probability. This is why it is so named. The other two learning functions can be interpreted similarly.

The best next point $\boldsymbol{u}^{(n+1)}$ at which to evaluate the $\mathcal{G}$-function can be chosen by maximizing the selected learning function such that:

$$\boldsymbol{u}^{(n+1)} = \arg\max_{\boldsymbol{u}\in\mathcal{U}} \mathrm{LF}(\boldsymbol{u}), \tag{41}$$

where $\mathrm{LF}(\boldsymbol{u})$ can refer to any of the three learning functions. The optimization problem involved in Eq. (41) can be solved by any suitable global optimization algorithm, e.g., genetic algorithm. In practice, it is unnecessary and infeasible to search the entire space $\mathcal{U}$ for a possible solution, and a reduced subspace could be sufficient, e.g., $[-R, R]^d$ with $R > 0$. In this study, the parameter R is specified by $R = \sqrt{\chi_d^{-2}(1-\rho)}$ with $\rho = 1 \times 10^{-10}$, where χ_d^2 is the CDF of a chi-squared distribution of degree d. Here, we will use the learning function 1 to illustrate why our active learning scheme works. By choosing the point that maximizes the $\mathrm{LSC}(\boldsymbol{u})$ function as the next point to query the $\mathcal{G}$-function, it is expected that the difference between $m_{P_{f,n+1}}$ and $\underline{m}_{P_{f,n+1}}$ will be reduced significantly. Besides, note from Eq. (38) that $\mathrm{LSC}(\boldsymbol{u})$ consists of the product of two terms. Obviously, the second term prefers the point whose joint PDF value is large. The first term favors the point where $\frac{m_{\mathcal{G}_n}(\boldsymbol{u})}{\sigma_{\mathcal{G}_n}(\boldsymbol{u})}$ equals $-\frac{b}{2}$ due to the property of Φ. This means that any point can be preferred, as long as the ratio between its posterior mean and standard deviation is a negative constant. From this perspective, the learning function $\mathrm{LSC}(\boldsymbol{u})$ allows a balance between exploration and exploitation through its first term. According to our computational experience, $b = 1$ might be a good choice.

3.3. Implementation procedure of the proposed methods

From the point of view of numerical implementation, the three proposed methods differ only in the stopping criterion and the learning function. For this reason, we will only present the implementation details of PBALC1, which involves six main steps and can be illustrated by the flowchart shown in Fig. 1.

Step 1: Generating an initial observation dataset

The first step involves generating an initial observation dataset by evaluating the $\mathcal{G}$-function. First, a small number (denoted as n_0) of uniformly distributed samples $\boldsymbol{\mathcal{U}} = \left\{\boldsymbol{u}^{(j)}\right\}_{j=1}^{n_0}$ are generated within a d-ball of radius R_0 by using the Sobol sequence. Herein, the radius R_0 is determined by $R_0 = \sqrt{\chi_d^{-2}(1-\rho_0)}$ with

$\rho_0 = 1 \times 10^{-8}$. Then, the output values $\boldsymbol{\mathcal{Y}} = \left[y^{(1)}, y^{(2)}, \cdots, y^{(n_0)}\right]^\top$ of the $\mathcal{G}$-function can be obtained, where $y^{(j)} = \mathcal{G}(\boldsymbol{u}^{(j)})$. At last, the initial observation dataset is formed as $\boldsymbol{\mathcal{D}} = \{\boldsymbol{\mathcal{U}}, \boldsymbol{\mathcal{Y}}\}$. Let $n = n_0$.

Step 2: Obtaining the posterior GP of the $\mathcal{G}$-function

At this stage, one needs to obtain the posterior GP ($\mathcal{GP}(m_{\mathcal{G}_n}(\boldsymbol{u}), k_{\mathcal{G}_n}(\boldsymbol{u}, \boldsymbol{u}'))$) of the $\mathcal{G}$-function conditional on the observation dataset $\boldsymbol{\mathcal{D}}$. This mainly involves tuning the hyper-parameters by the use of maximum likelihood estimation. In this study, we adopt the *fitrgp* function in the Statistics and Machine Leaning Toolbox of Matlab.

Step 3: Computing the two terms in the stopping criterion

The two estimates $\hat{m}_{P_{f,n}}$ and $\hat{\underline{\Delta}}_{P_{f,n}}$ that will be used in the stopping criterion are computed by using the sequential VAIS technique, as described in subsection 3.1.

Step 4: Checking the stopping criterion

If the stopping criterion, $\frac{\hat{\underline{\Delta}}_{P_{f,n}}}{\hat{m}_{P_{f,n}}} < \epsilon_1$ is satisfied twice in a row, go to **Step 6**; Else, go to **Step 5**.

Step 5: Enriching the observation dateset

The best next point to evaluate the $\mathcal{G}$-function is identified by maximizing the LSC($\boldsymbol{u}$) function such that $\boldsymbol{u}^{(n+1)} = \arg\max_{\boldsymbol{u} \in [-R,R]^d} \text{LSC}(\boldsymbol{u})$. After that, the $\mathcal{G}$-function is evaluated at $\boldsymbol{u}^{(n+1)}$ to produce the corresponding output value $y^{(n+1)}$. The previous dataset $\boldsymbol{\mathcal{D}}$ is enriched with $\left\{\boldsymbol{u}^{(n+1)}, y^{(n+1)}\right\}$. Let $n = n+1$, and go to **Step 2**.

Step 6: Ending the algorithm

Return $\hat{m}_{P_{f,n}}$ as the failure probability estimate and end the algorithm.

4. Numerical examples

This section investigates five numerical examples to demonstrate the performance of the three proposed methods, namely PBALC1, PBALC2 and PBALC3. The unspecified parameters involved are set as follows: $n_0 = 10$, $b = 1$, $\lambda = 2$, $N_0 = 10^6$, $\delta_1 = 2\%$, $\delta_2 = 5\%$, $\epsilon_1 = 2.5\%(5\%)$, $\epsilon_2 = 2.5\%(5\%)$, $\epsilon_3 = 5\%(10\%)$. The reference failure probability for each example is obtained from the crude MCS with a sufficiently large number of samples, if applicable. For comparison purposes, three state-of-the-art methods, Active Learning

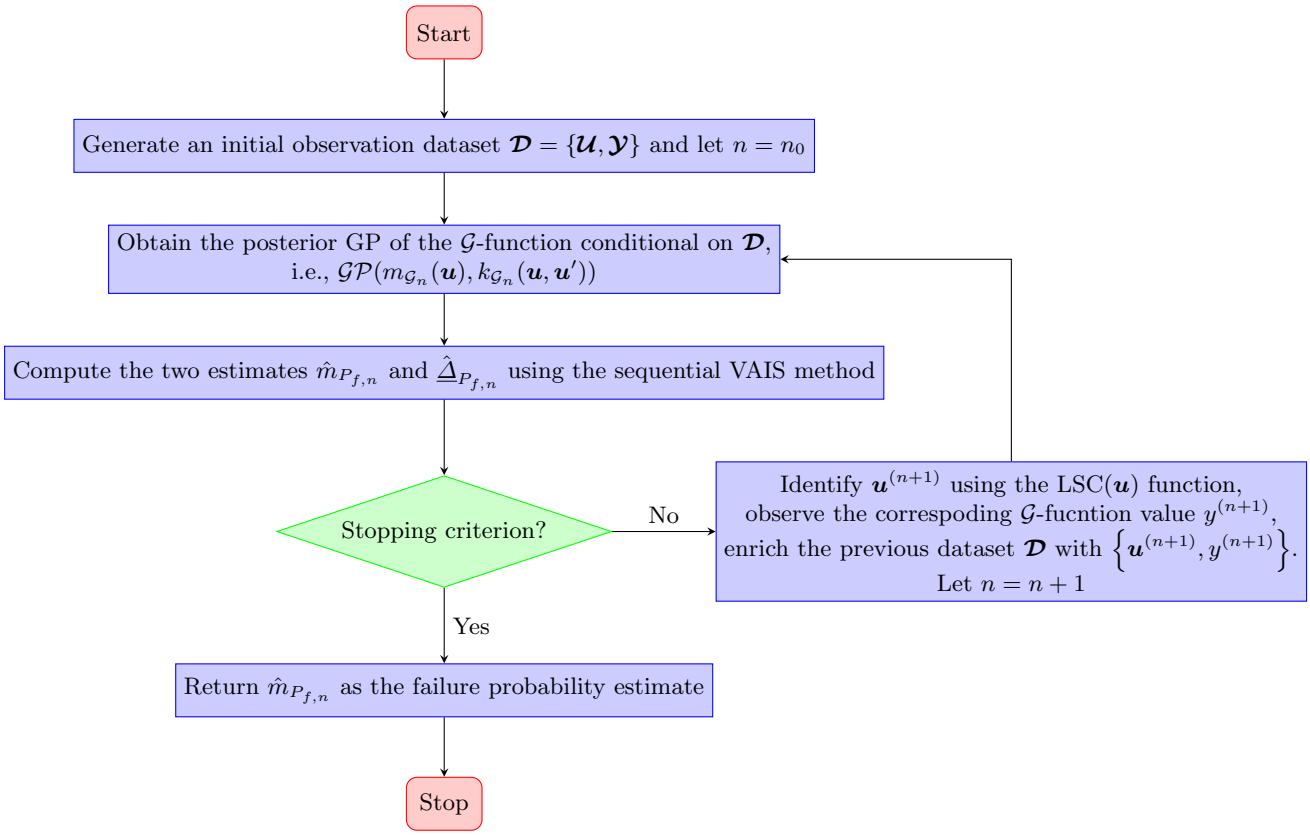

Figure 1: Flowchart of the proposed PBALC1 method.

Kriging Markov Chain Monte Carlo (AK-MCMC) [28], Active Learning Kriging-Kernel Density Estimation-Importance Sampling (ALK-KDE-IS) [29] and Bayesian Subset Simulation (BSS) [30], are also implemented in all examples. All methods except MCS (or its substitute) are run 20 independent times to test their robustness, and the average results are reported.

4.1. Example 1: A series system with four branches

The first example considers a series system with four branches, which has been a common benchmark for the verification of structural reliability analysis methods [20]. The performance function is given by:

$$g\left(X_1, X_2\right) = \min \begin{cases} a + \frac{(X_1 - X_2)^2}{10} - \frac{(X_1 + X_2)}{\sqrt{2}} \\ a + \frac{(X_1 - X_2)^2}{10} + \frac{(X + X_2)}{\sqrt{2}} \\ (X_1 - X_2) + \frac{b}{\sqrt{2}} \\ (X_2 - X_1) + \frac{b}{\sqrt{2}} \end{cases}, \tag{42}$$

where X_1 and X_2 are two independent standard normal variables; a and b are two constant parameters, which are specified as 6 and 12, respectively.

Table 1 summarizes the results obtained by several methods, i.e., MCS, AK-MCMC, ALK-KDEIS, BSS, PBALC1, PBALC2 and PBALC3. The reference value of the failure probability is 3.01×10^{-9} with a COV of 1.82%, given by the crude MCS with 10^{12} samples. AK-MCMC produces an average failure probability (say 2.34×10^{-9}) that is smaller than the reference value and with a large COV (say 33.11%), implying its inaccuracy in this example. However, it requires an average of 195.45 performance function evaluations, which is the most of the six competing methods. At the cost of 84.10 $\mathcal{G}$-function calls on average, ALK-KDE-IS can produce an unbiased result for the failure probability with a COV of 0.55%. As for BSS, it generates a biased result for the failure probability with a very large COV (i.e., 47.64%), even at the cost of an average of 66.35 performance function evaluations. On the contrary, all three proposed methods are capable of producing fairly accurate failure probabilities with an average of only about $45 \sim 50$ performance function evaluations. Among them, PBALC1 requires the fewest $\mathcal{G}$-function calls on average, but has the largest COV.

To further illustrate the proposed methods, we show in Figs. 2-4 the learning curves (left panel) and selected points (right panel) generated from an exemplary run of the three methods. From the learning curves, we can see that the posterior mean estimate of the failure probability $\hat{m}_{P_{f,n}}$ eventually approaches the reference failure probability. Also, the left-shifted and right-shifted posterior mean estimates of the

Table 1: Reliability analysis results of Example 1 obtained by several methods.

Method	$\hat{P}_f$	COV $\left[\hat{P}_f\right]$	N_{call}
MCS	3.01×10^{-9}	1.82%	10^{12}
AK-MCMC	2.34×10^{-9}	33.11%	195.45
ALK-KDE-IS	3.03×10^{-9}	0.55%	84.10
BSS	3.52×10^{-9}	47.64%	66.35
Proposed PBALC1 ($\epsilon_1 = 2.5\%$)	3.04×10^{-9}	3.82%	44.75
Proposed PBALC2 ($\epsilon_2 = 2.5\%$)	3.04×10^{-9}	1.39%	50.10
Proposed PBALC3 ($\epsilon_3 = 5\%$)	3.03×10^{-9}	1.99%	49.50

failure probability ($\underline{\hat{m}}_{P_{f,n}}$ and $\overline{\hat{m}}_{P_{f,n}}$) gradually approach $\hat{m}_{P_{f,n}}$. On the other hand, it can be observed from the selected points that most of the added points are close to the four important parts of the limit state curve that are crucial for the failure probability estimation.

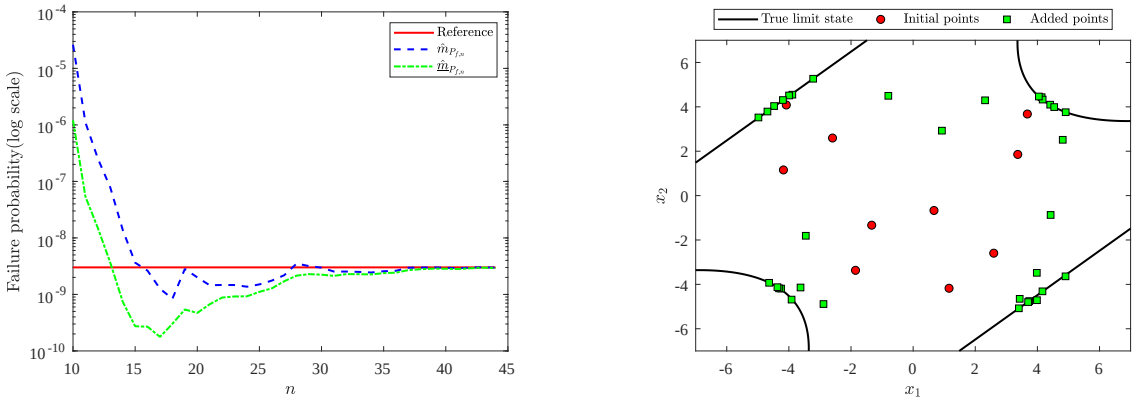

(a) Learning curves (b) Selected points

Figure 2: Illustration of the proposed PBALC1 method for Example 1.

4.2. Example 2: A nonlinear oscillator

As a second example, we consider a nonlinear, undamped, single-degree-of-freedom (SDOF) oscillator subject to a rectangular pulse load [31], as shown in Fig 5. The performance function is formulated as:

$$g\left(m, k_1, k_2, r, F_1, t_1\right) = 3r - \left| \frac{2F_1}{k_1 + k_2} \sin\left(\frac{t_1}{2} \sqrt{\frac{k_1 + k_2}{m}} \right) \right|, \tag{43}$$

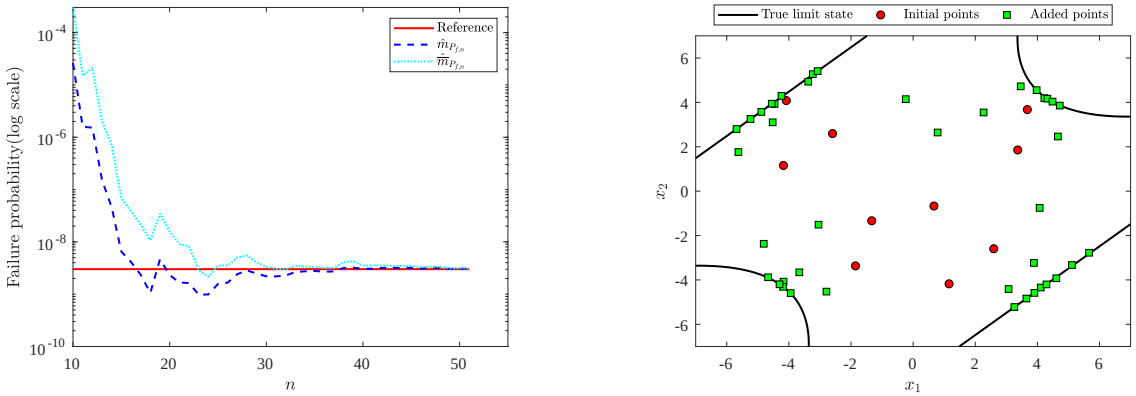

(a) Learning curves (b) Selected points

Figure 3: Illustration of the proposed PBALC2 method for Example 1.

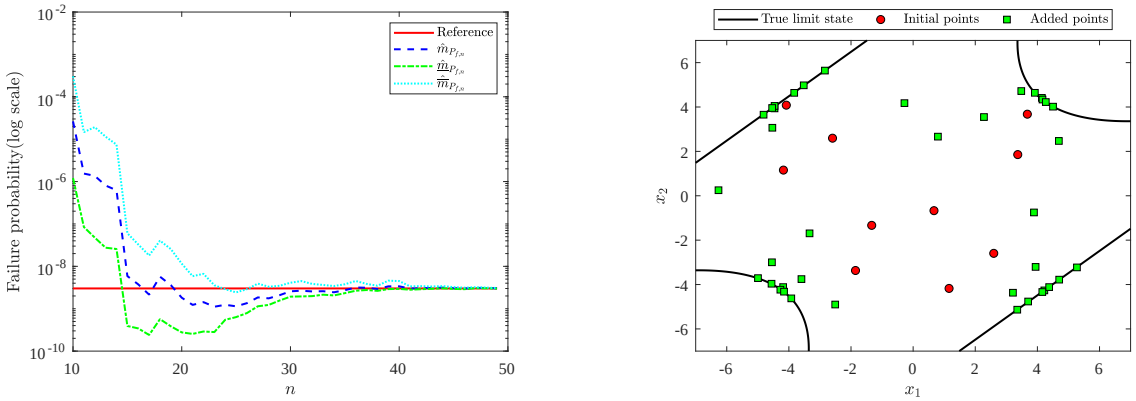

(a) Learning curves (b) Selected points

Figure 4: Illustration of the proposed PBALC3 method for Example 1.

where m, k_1, k_2, r, F_1 and t_1 are six random variables, as detailed in Table 2.

The proposed three methods are compared in Table 3 with several other reliability analysis methods, i.e., MCS, AK-MCMC, ALK-KDE-IS and BSS. With 10^{12} samples, MCS can produce a failure probability estimate of 4.01×10^{-8} with a rather small COV (say 0.50%), so it is used as a reference solution. All the other six methods except BSS are able to give quite good results. However, the three proposed methods significantly outperform other methods in terms of the average number of performance function calls. Note that PBALC1 has a sightly larger COV and requires a sightly fewer $\mathcal{G}$-function calls on average than PBALC2 and PBALC3.

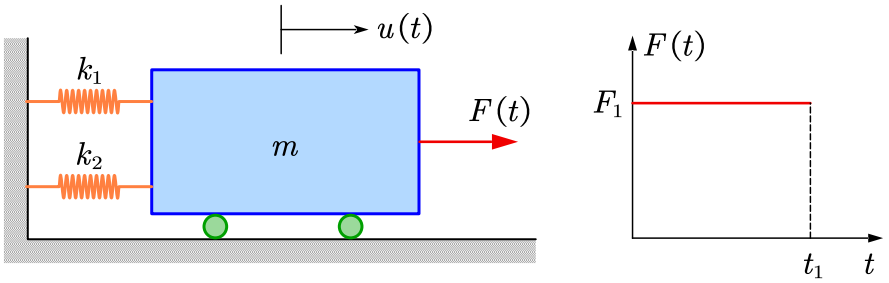

Figure 5: A nonlinear SDOF oscillator under a rectangular pulse load.

Table 2: Random variables for Example 2.

Variable	Description	Distribution	Mean	COV
m	Mass	Lognormal	1.0	0.05
k_1	Stiffness	Lognormal	1.0	0.10
k_2	Stiffness	Lognormal	0.2	0.10
r	Yield displacement	Lognormal	0.5	0.10
F_1	Load amplitude	Lognormal	0.4	0.20
t_1	Load duration	Lognormal	1.0	0.20

4.3. Example 3: An I beam

The third example involves a simply-supported I beam subjected to a concentrated force [32], as depicted in Fig. 6. The performance function is expressed as:

$$g(\boldsymbol{X}) = S - \sigma_{\max}, \tag{44}$$

in which

$$\sigma_{\max} = \frac{Pa(L-a)d}{2LI}, \tag{45}$$

with

$$I = \frac{b_f d^3 - (b_f - t_w)(d - 2t_f)^3}{12}. \tag{46}$$

In this example, a total of eight random variables are considered, as listed in the table 4.

Table 3: Reliability analysis results of Example 2 obtained by several methods.

Method	$\hat{P}_f$	COV $\left[\hat{P}_f\right]$	N_{call}
MCS	4.01×10^{-8}	0.50%	10^{12}
AK-MCMC	4.03×10^{-8}	0.76%	282.30
ALK-KDE-IS	4.03×10^{-8}	2.92%	84.60
BSS	4.53×10^{-8}	32.53%	77.75
Proposed PBALC1 ($\epsilon_1 = 5\%$)	4.03×10^{-8}	4.29%	29.10
Proposed PBALC2 ($\epsilon_2 = 5\%$)	4.07×10^{-8}	2.61%	31.90
Proposed PBALC3 ($\epsilon_2 = 10\%$)	4.05×10^{-8}	3.66%	30.95

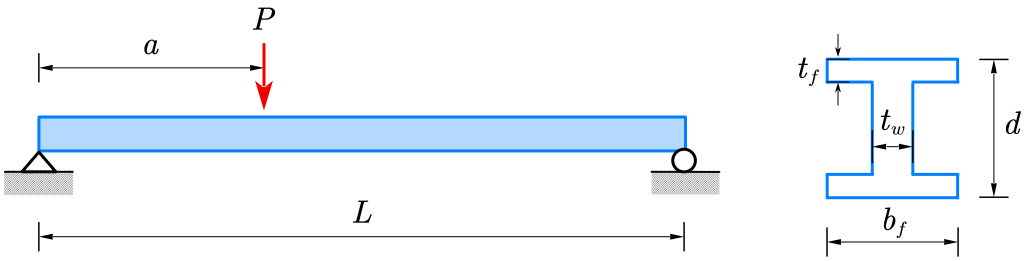

Figure 6: A simply-supported I beam subjected to a concentrated force.

Table 5 reports the reliability analysis results by several methods. The reference value of the failure probability is 1.69×10^{-7} with a COV of 0.77%, provided by MCS with 10^{11} samples. At the cost of an average of 376.70 performance function evaluations, AK-MCMC can produce an unbiased result for the failure probability with a small COV. The results of ALK-KDE-IS are missing because it cannot converge in multiple trials. BSS still gives a slightly biased result, even with 104.90 $\mathcal{G}$-function calls on average. On the contrary, with an average of about 45-46 performance evaluations, the three proposed methods are able to produce desired results.

Table 4: Random variables for Example 3.

Variable	Distribution	Mean	COV
P	Lognormal	1500	0.20
L	Normal	120	0.05
a	Normal	72	0.10
S	Normal	200,000	0.15
d	Normal	2.3	0.05
b_f	Normal	2.3	0.05
t_w	Normal	0.16	0.05
t_f	Normal	0.26	0.05

4.4. Example 4: A spatial truss

As a fourth example to illustrate the performance of the proposed methods, we consider a 56-bar space truss structure [33], which is shown in Fig. 7. The structure is modelled as a three-dimensional finite element model with 35 nodes and 56 truss elements using OpenSees. Nine vertical concentrated forces, $P_1 \sim P_9$, are applied to the model along the negative of the z-axis. The cross-sectional area and Young's modulus of each element are assumed to be the same and denoted as A and E respectively. The performance function is defined as:

$$g(P_1 \sim P_9, E, A) = \Delta - V_1(P_1 \sim P_9, E, A), \tag{47}$$

where V_1 is the displacement of node 1 along the negative of the z-axis; Δ is the threshold, which is set to be 50 mm; $P_1 \sim P_9$, E and A are 11 random variables, as listed in Table 6.

To obtain a reference solution for the failure probability, we implement the importance sampling (IS) method available in UQLab [34]. The results of several other methods are reported in Table 7, as well as the IS method. The failure probability estimate produced by IS is 4.83×10^{-8} with a COV of 0.99%, at the cost of 67,107 g-function evaluations. Although AK-MCMC can produce an unbiased result, it has a COV up to 9.33% and requires an average of 453.80 model evaluations. At the cost of 176.45 $\mathcal{G}$-function calls,

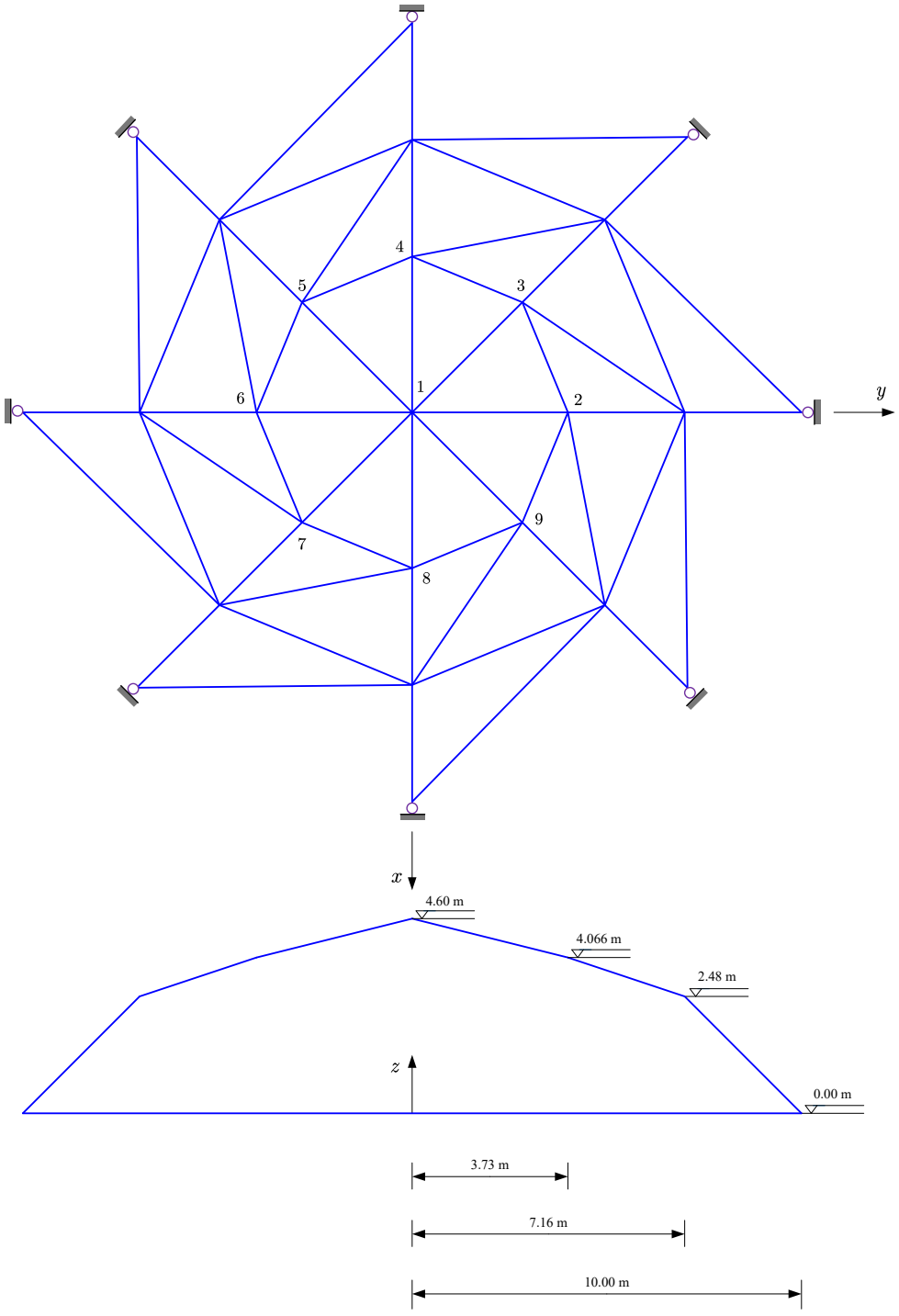

Figure 7: Schematic of a 56-bar space truss structure.

Table 5: Reliability analysis results of Example 3 obtained by several methods.

Method	$\hat{P}_f$	COV $\left[\hat{P}_f\right]$	N_{call}
MCS	1.69×10^{-7}	0.77%	10^{11}
AK-MCMC	1.71×10^{-7}	2.13%	376.70
ALK-KDE-IS	-	-	-
BSS	1.88×10^{-7}	31.38%	104.90
Proposed PBALC1 ($\epsilon_1 = 5\%$)	1.69×10^{-7}	3.14%	45.05
Proposed PBALC2 ($\epsilon_2 = 5\%$)	1.67×10^{-7}	4.08%	45.00
Proposed PBALC3 ($\epsilon_3 = 10\%$)	1.69×10^{-7}	2.71%	46.70

Table 6: Random variables for Example 4.

Variable	Distribution	Mean	COV
P_1	Lognormal	150 kN	0.20
$P_2 \sim P_9$	Lognormal	100 kN	0.20
E	Normal	2.06 GPa	0.10
A	Normal	2,000 mm^2	0.05

ALK-KDE-IS produces a biased result with a considerably large COV (i.e., 24.06%). As for BSS, a biased result can be produced using an average of 81.70 $\mathcal{G}$-function calls. It is noteworthy that the three proposed methods only require on average less than 30 model evaluations, while still maintaining a desired level of accuracy.

4.5. Example 5: A dam seepage model

The last example involves the study of the steady-state confined seepage flow below a dam (adopted from [35]), as shown in Fig. 8. The dam foundation consists of an impermeable layer and two permeable layers (silty sand and silty gravel). A cut-off wall is installed at the bottom of the dam to prevent excessive seepage. The upstream water has a height of h_D m. Thus, the hydraulic h_W over the impermeable layer is $h_W = h_D + 20$ m. It is assumed that the water only flows from the segment AB to the segment CD

Table 7: Reliability analysis results of Example 4 obtained by several methods.

Method	$\hat{P}_f$	COV $\left[\hat{P}_f\right]$	N_{call}
IS	4.83×10^{-8}	0.99%	67,107
AK-MCMC	4.83×10^{-8}	9.33%	453.80
ALK-KDE-IS	4.52×10^{-8}	24.06%	176.45
BSS	5.34×10^{-8}	24.90%	81.70
Proposed PBALC1 ($\epsilon_1 = 5\%$)	4.86×10^{-8}	5.70%	27.20
Proposed PBALC2 ($\epsilon_2 = 5\%$)	4.85×10^{-8}	4.61%	26.90
Proposed PBALC3 ($\epsilon_3 = 10\%$)	4.87×10^{-8}	6.64%	26.30

through the two permeable layers (where the the vertical and horizontal permeabilities of the i-th layer are denoted as $k_{xx,i}$ and $k_{yy,i}$, respectively). Five quantities (i.e., h_D, $k_{xx,1}$, $k_{yy,1}$, $k_{xx,2}$ and $k_{yy,2}$) are considered as random variables, as given in Table 8. The hydraulic head of the seepage problem is governed by the following partial differential equation:

$$k_{xx,i}\frac{\partial^2 h_W}{\partial x^2} + k_{yy,i}\frac{\partial^2 h_W}{\partial y^2} = 0, i = 1, 2. \tag{48}$$

The equation is numerically solved by using the finite element method with 1628 quadratic triangular elements, as depicted in Fig. 9. Once h_W is solved, the seepage discharge q at the downstream side of the dam, measured in units of volume over time over distance, can be calculated:

$$q = -\int_{\mathrm{CD}} k_{yy,2}\frac{\partial h_W}{\partial y}\mathrm{d}x. \tag{49}$$

The performance function of this problem is formulated as:

$$g(h_D, k_{xx,1}, k_{yy,1}, k_{xx,2}, k_{yy,2}) = \Delta - q(h_D, k_{xx,1}, k_{yy,1}, k_{xx,2}, k_{yy,2}), \tag{50}$$

where Δ denotes a prescribed threshold for the seepage discharge q, which is set as 20 L/h/m.

Table 9 lists the results of several reliability analysis methods. The reference value for the failure probability is adopted as 7.78×10^{-6}, given by the IS method in UQLab [34]. With an average of 94.75 performance function evaluations, AK-MCMC gives a failure probability mean that is close to the reference

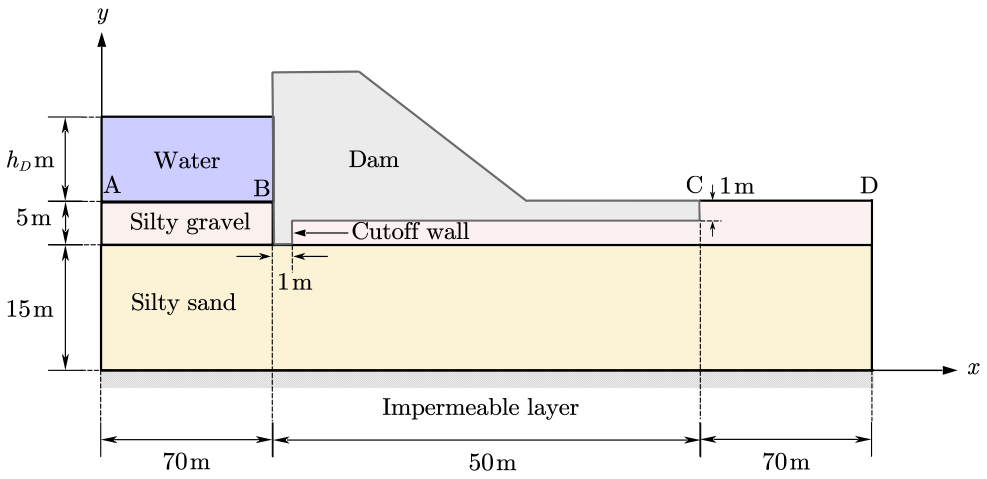

Figure 8: Schematic illustration of the dam seepage problem.

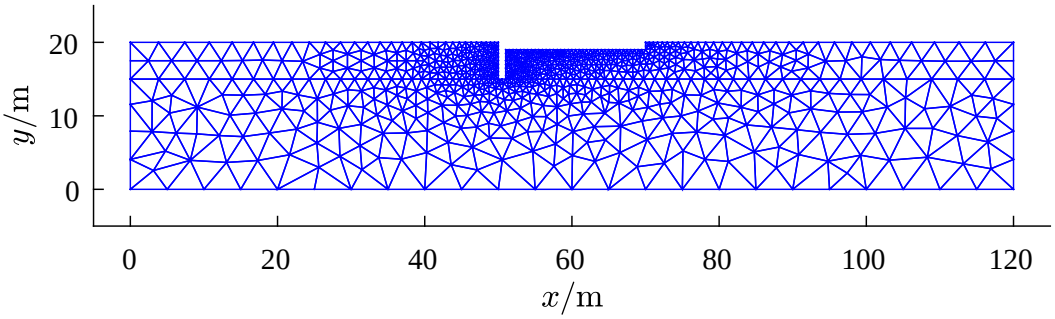

Figure 9: Finite-element mesh of the permeable layers.

one, while processing a small COV. ALK-KDE-IS requires more $\mathcal{G}$ function calls on average than AK-MCMC, but has slightly larger variability. The COV of the BSS is as high as 27.40%, even though the average number of model evaluations is only 43.85. All the three proposed PBALC methods can produce fairly good results for the failure probability at the cost of up to 77.55 performance function calls (average). Note that PBALC1 requires relatively fewer model evaluations than PBALC2 and PBALC3 on average in this example.

Remark: The three proposed methods perform very similarly in all five numerical examples, except for the first and last two (where PBALC1 is clearly more efficient, but exhibits relatively larger variability in example 1). Therefore, PBALC1 is recommended when efficiency is more important than accuracy, and vice

Table 8: Random variables for Example 5.

Variable	Distribution	Parameter 1	Parameter 2
h_D (m)	Uniform	7	10
$k_{xx,1}$ (10^{-7}m/s)	Gumbel	5	0.20
$k_{yy,1}$ (10^{-7}m/s)	Gumbel	2	0.20
$k_{xx,2}$ (10^{-6}m/s)	Lognormal	5	0.20
$k_{yy,2}$ (10^{-6}m/s)	Lognormal	2	0.20

Note: Parameter 1 and Parameter 2 denote the lower and upper bounds for a uniform distribution, while mean and COV for a Gumbel/Lognormal distribution, respectively.

versa.

5. Concluding remarks

This study presents three novel Bayesian active learning methods under the name 'partially Bayesian active learning cubature' (PBALC) for structural reliability analysis, especially when small failure probabilities are involved. These methods are the result of extending the framework of Bayesian failure probability inference to Bayesian active learning of failure probabilities. The basic idea is to use only the posterior mean of the failure probability to design the stopping criterion and the learning function. Following this idea, we creatively propose three stopping criteria by exploring the structure of the posterior mean of the failure probability. In addition, the analytically intractable integrals encountered in the stopping criteria are numerically approximated by the sequential variance-amplified importance sampling, which also enables to assess very small failure probabilities. Motivated by the stopping criteria, we further develop three learning functions that allow a balance between exploration and exploitation. The three stopping criteria and associated learning functions correspond to the three proposed methods PBALC1, PBALC2 and PBALC3. Numerical studies show that these proposed methods can accurately evaluate very small failure probabilities

Table 9: Reliability analysis results of Example 5 obtained by several methods.

Method	$\hat{P}_f$	COV $\left[\hat{P}_f\right]$	N_{call}
IS	7.78×10^{-6}	1.97%	16,218
AK-MCMC	7.78×10^{-6}	0.80%	94.75
ALK-KDE-IS	7.76×10^{-6}	2.55%	125.00
BSS	7.73×10^{-6}	27.40%	43.85
Proposed PBALC1 ($\epsilon_1 = 5\%$)	7.76×10^{-6}	1.74%	62.60
Proposed PBALC2 ($\epsilon_2 = 5\%$)	7.82×10^{-6}	1.88%	76.40
Proposed PBALC3 ($\epsilon_3 = 10\%$)	7.81×10^{-6}	1.81%	77.55

in the order of 10^{-6} - 10^{-9}. Besides, they also significantly outperform several existing methods in the literature in terms of accuracy and efficiency.

The proposed methods are expected to be applicable to weakly and moderately nonlinear problems in low to medium dimensions. For highly nonlinear and/or high-dimensional problems (e.g., dynamic reliability analysis of nonlinear structures under random excitation), special treatments are required. In addition, some minor efforts could be made in the future along the following directions. The sequential variance-amplified importance sampling is found to be time-consuming in some cases, though it is a robust method for numerically approximating the analytically intractable integrals involved in the proposed stopping criteria. Therefore, an interesting future direction is to develop a more refined importance sampling instead. In addition, we select only a single point that maximizes the learning functions at the active learning phase, which may waste other useful information and does not support parallel distributed processing. In the future, a multi-point selection strategy can be developed to reduce the number of performance function evaluations and enable parallel computing.

Declaration of competing interest

The authors declare that they have no known competing financial interests or personal relationships that could have appeared to influence the work reported in this paper.

Acknowledgments

Chao Dang is mainly supported by China Scholarship Council (CSC). Pengfei Wei is grateful to the support from the National Natural Science Foundation of China (grant no. 51905430 and 72171194).

Data availability

Data will be made available on request.

References

[1] N. Kurtz, J. Song, Cross-entropy-based adaptive importance sampling using gaussian mixture, Structural Safety 42 (2013) 35–44. doi:https://doi.org/10.1016/j.strusafe.2013.01.006.

[2] I. Papaioannou, C. Papadimitriou, D. Straub, Sequential importance sampling for structural reliability analysis, Structural Safety 62 (2016) 66–75. doi:https://doi.org/10.1016/j.strusafe.2016.06.002.

[3] S.-K. Au, J. L. Beck, Estimation of small failure probabilities in high dimensions by subset simulation, Probabilistic Engineering Mechanics 16 (4) (2001) 263–277. doi:https://doi.org/10.1016/S0266-8920(01)00019-4.

[4] S.-K. Au, Y. Wang, Engineering risk assessment with subset simulation, John Wiley & Sons, 2014.

[5] P. Bjerager, Probability integration by directional simulation, Journal of Engineering Mechanics 114 (8) (1988) 1285–1302. doi:https://doi.org/10.1061/(ASCE)0733-9399(1988)114:8(1285).

[6] J. Nie, B. R. Ellingwood, Directional methods for structural reliability analysis, Structural Safety 22 (3) (2000) 233–249. doi:https://doi.org/10.1016/S0167-4730(00)00014-X.

[7] P.-S. Koutsourelakis, H. J. Pradlwarter, G. I. Schueller, Reliability of structures in high dimensions, part i: algorithms and applications, Probabilistic Engineering Mechanics 19 (4) (2004) 409–417. doi:https://doi.org/10.1016/j.probengmech.2004.05.001.

[8] K. W. Breitung, Asymptotic approximations for probability integrals, Springer, 2006.

[9] A. M. Hasofer, N. C. Lind, Exact and invariant second-moment code format, Journal of the Engineering Mechanics Division 100 (1) (1974) 111–121. doi:https://doi.org/10.1061/JMCEA3.0001848.

[10] K. Breitung, Asymptotic approximations for multinormal integrals, Journal of Engineering Mechanics 110 (3) (1984) 357–366. doi:https://doi.org/10.1061/(ASCE)0733-9399(1984)110:3(357).

[11] Y.-G. Zhao, T. Ono, Moment methods for structural reliability, Structural Safety 23 (1) (2001) 47–75. doi:https://doi.org/10.1016/S0167-4730(00)00027-8.

[12] J. Xu, C. Dang, A new bivariate dimension reduction method for efficient structural reliability analysis, Mechanical Systems and Signal Processing 115 (2019) 281–300. doi:https://doi.org/10.1016/j.ymssp.2018.05.046.

[13] X. Zhang, M. D. Pandey, Structural reliability analysis based on the concepts of entropy, fractional moment and dimensional reduction method, Structural Safety 43 (2013) 28–40. doi:https://doi.org/10.1016/j.strusafe.2013.03.001.

[14] J. Xu, F. Kong, Adaptive scaled unscented transformation for highly efficient structural reliability analysis by maximum entropy method, Structural Safety 76 (2019) 123–134. doi:https://doi.org/10.1016/j.strusafe.2018.09.001.

[15] J. Li, J.-b. Chen, W.-l. Fan, The equivalent extreme-value event and evaluation of the structural system reliability, Structural Safety 29 (2) (2007) 112–131. doi:https://doi.org/10.1016/j.strusafe.2006.03.002.

[16] K. Gao, G. Liu, W. Tang, High-dimensional reliability analysis based on the improved number-theoretical method, Applied Mathematical Modelling 107 (2022) 151–164. doi:https://doi.org/10.1016/j.apm.2022.02.030.

[17] X. Li, G. Chen, H. Cui, D. Yang, Direct probability integral method for static and dynamic reliability analysis of structures with complicated performance functions, Computer Methods in Applied Mechanics and Engineering 374 (2021) 113583. doi:https://doi.org/10.1016/j.cma.2020.113583.

[18] G. Chen, D. Yang, A unified analysis framework of static and dynamic structural reliabilities based on direct probability integral method, Mechanical Systems and Signal Processing 158 (2021) 107783. doi:https://doi.org/10.1016/j.ymssp.2021.107783.

[19] B. J. Bichon, M. S. Eldred, L. P. Swiler, S. Mahadevan, J. M. McFarland, Efficient global reliability analysis for nonlinear implicit performance functions, AIAA Journal 46 (10) (2008) 2459–2468.

[20] B. Echard, N. Gayton, M. Lemaire, AK-MCS: an active learning reliability method combining Kriging and Monte Carlo simulation, Structural Safety 33 (2) (2011) 145–154. doi:https://doi.org/10.1016/j.strusafe.2011.01.002.

[21] F.-X. Briol, C. J. Oates, M. Girolami, M. A. Osborne, D. Sejdinovic, Probabilistic Integration: A Role in Statistical Computation?, Statistical Science 34 (1) (2019) 1 – 22. doi:https://doi.org/10.1214/18-STS660.

[22] C. Dang, P. Wei, J. Song, M. Beer, Estimation of failure probability function under imprecise probabilities by active learning–augmented probabilistic integration, ASCE-ASME Journal of Risk and Uncertainty in Engineering Systems, Part A: Civil Engineering 7 (4) (2021) 04021054. doi:https://doi.org/10.1061/AJRUA6.0001179.

[23] C. Dang, P. Wei, M. G. Faes, M. A. Valdebenito, M. Beer, Parallel adaptive bayesian quadrature for rare event estimation, Reliability Engineering & System Safety 225 (2022) 108621. doi:https://doi.org/10.1016/j.ress.2022.108621.

[24] C. Dang, M. A. Valdebenito, M. G. Faes, P. Wei, M. Beer, Structural reliability analysis: A Bayesian perspective, Structural Safety 99 (2022) 102259. doi:https://doi.org/10.1016/j.strusafe.2022.102259.

[25] Z. Hu, C. Dang, L. Wang, M. Beer, Parallel bayesian probabilistic integration for structural reliability analysis with small failure probability, Submitted to Structural Safety (2023).

[26] C. Dang, M. A. Valdebenito, J. Song, P. Wei, M. Beer, Estimation of small failure probabilities by partially Bayesian active learning line sampling: Theory and algorithm, Computer Methods in Applied Mechanics and Engineering 412 (2023) 116068. doi:https://doi.org/10.1016/j.cma.2023.116068.

[27] C. Dang, M. A. Valdebenito, M. G. Faes, J. Song, P. Wei, M. Beer, Structural reliability analysis by line sampling: A Bayesian active learning treatment, Structural Safety 104 (2023) 102351. doi:https://doi.org/10.1016/j.strusafe.2023.102351.

[28] P. Wei, C. Tang, Y. Yang, Structural reliability and reliability sensitivity analysis of extremely rare failure events by combining sampling and surrogate model methods, Proceedings of the Institution of Mechanical Engineers, Part O: Journal of Risk and Reliability 233 (6) (2019) 943–957. doi:https://doi.org/10.1177/1748006X19844666.

[29] X. Yang, Y. Liu, C. Mi, X. Wang, Active learning kriging model combining with kernel-density-estimation-based importance sampling method for the estimation of low failure probability, Journal of Mechanical Design 140 (5) (2018) 051402. doi:https://doi.org/10.1115/1.4039339.

[30] J. Bect, L. Li, E. Vazquez, Bayesian subset simulation, SIAM/ASA Journal on Uncertainty Quantification 5 (1) (2017) 762–786. doi:https://doi.org/10.1137/16M1078276.

[31] C. G. Bucher, U. Bourgund, A fast and efficient response surface approach for structural reliability problems, Structural Safety 7 (1) (1990) 57–66. doi:https://doi.org/10.1016/0167-4730(90)90012-E.

[32] B. Huang, X. Du, Uncertainty Analysis by Dimension Reduction Integration and Saddlepoint Approximations, Journal of Mechanical Design 128 (1) (2005) 26–33. doi:https://doi.org/10.1115/1.2118667.

[33] C. Dang, P. Wei, M. G. Faes, M. Beer, Bayesian probabilistic propagation of hybrid uncertainties: Estimation of response expectation function, its variable importance and bounds, Computers & Structures 270 (2022) 106860. doi:https://doi.org/10.1016/j.compstruc.2022.106860.

[34] S. Marelli, R. Schöbi, B. Sudret, UQLab user manual – Structural reliability (Rare event estimation), Tech. rep., Chair of Risk, Safety and Uncertainty Quantification, ETH Zurich, Switzerland, report UQLab-V2.0-107 (2022).

[35] M. A. Valdebenito, H. A. Jensen, H. Hernández, L. Mehrez, Sensitivity estimation of failure probability applying line sampling, Reliability Engineering & System Safety 171 (2018) 99–111. doi:https://doi.org/10.1016/j.ress.2017.11.010.